Effect of Pilot Fuel-staging Ratio on Swirling Combustor Performance

Liyao Pang[1], Xu Cheng[2], Honghao Xu[1], Zongfu Li[1], Xiaotao Yang[1], Ningbo Zhao[1]
[1]College of Power and Energy Engineering/Harbin Engineering University
145 Nantong Street Nangang District, Harbin, China
pangliyao030006@hrbeu.edu.cn; xuhonghaocn@163.com; 15776454460@163.com
yangxiaotao1985@163.com; zhaoningboheu@126.com
[2]NO.703 Research Institute/China State Shipbuilding Corporation
Harbin, China
2595526@163.com

Abstract - With the transition towards higher temperature rise and increased fuel-air ratio, combustor design faces a series of challenges. The centrally-staged combustion approach, as a widely adopted strategy in high-temperature-rise combustor design, resolves the inherent conflict between lean blowout at a low-power condition and visible smoke at a high-power condition by coordinating the main and pilot stages. Fuel supply and distribution affect the flame position, temperature distribution, and overall performance of the combustor. In this work, numerical simulations evaluate the effect of the pilot stage fuel-staging ratio on a single-sector centrally-staged high-temperature-rise combustor using kerosene under high-power conditions. With the main and pilot stage swirler structures remaining unchanged, the effects of varying pilot stage fuel-staging ratio on swirling combustion flow characteristics, flame morphology, temperature distribution, and emission characteristics are analysed. The main results indicate that the influence of the inner shear layer causes fuel stratification between the main and pilot stages, leading to a V-shaped fuel distribution within the combustor. The flame likewise exhibits layering, with the main flame front extending along the edge of the lip recirculation zone and remaining minimally affected by variations in the pilot stage fuel-staging ratio. The pilot flame is located at the edge of the fuel distribution contour within the primary recirculation zone. As the pilot stage fuel-staging ratio increases, the axial distance between the pilot flame front and the swirler exit elongates, while the heat release zone simultaneously expands. Increased pilot stage fuel flow rate enlarges the high-temperature zone, leading to higher CO emissions. With the pilot stage fuel-staging ratio increasing from 10% to 70%, CO emissions rise more than threefold, total pressure loss coefficient fluctuates slightly, combustion efficiency continuously declines, and the outlet temperature distribution coefficient remains high, reflecting a deterioration in overall combustor performance.

Keywords: high temperature rise; centrally-staged combustor; fuel-staging ratio; combustion flow field; flame morphology

1. Introduction

Achieving a high thrust-to-weight ratio is a primary objective for the development of future advanced aircraft engines [1]. In terms of engine simple cycle performance, increasing unit thrust by elevating the turbine inlet temperature is the most direct and effective method to enhance the thrust-to-weight ratio, compared to increasing the pressure ratio [2]. Consequently, combustors are trending towards higher temperature rise and higher fuel-air ratio (FAR), which introduces a series of challenges in combustor design [3]. Notably, lean blowout (LBO) or combustion instability due to increased air intake at low-power operating conditions and visible smoke resulting from excessively high FAR at high-power operating conditions have emerged as a fundamental challenge in the design of high-temperature-rise (HTR) combustors. The centrally-staged combustion organization method can mitigate the inherent contradiction of "LBO and excessive smoke" through the coordination of the main and pilot stages, which is a strategy widely employed in the design of HTR combustors.

Currently, extensive researches on centrally-staged HTR combustors have been conducted by numerous scholars. Suo et al. [4] investigated the LBO characteristics of a centrally-staged single flame tube combustor through experiments, revealing that the LBO FAR decreases as the inlet pressure increases. Ge et al. [5] explored the impact of pilot stage structures on the flow characteristics of centrally-staged HTR combustors using large eddy simulation. The results show that as the swirling number of the pilot stage increases, the primary recirculation zone (PRZ) progressively lengthens and widens. Wang et al. [6] adjusted the swirling vane installation angle to control the outlet temperature field of centrally-staged HTR

combustors. The findings demonstrate that increasing the swirling number pushes the flame front and high-temperature zone downstream within the combustor, which enhances mixing, improves heat transfer, and reduces the temperature distribution coefficient at the outlet. Sun et al. [7] numerically examined the impact of fuel supply distribution on the performance of centrally-staged HTR combustors. The results indicate that the main fuel distribution significantly affects the temperature field, with increased fuel allocation improving combustion efficiency and enhancing the uniformity of the outlet temperature field. A substantial number of previous reviews have focused on the performance of centrally-staged HTR or high FAR combustors, particularly concerning the stage structure within the swirler, the fuel supply method, and the fuel-staging ratio (FSR). The stage structure affects the swirling combustion flow field and flame structure [8], while the fuel supply method and FSR influence the flame position [9], which in turn impacts the temperature distribution and combustor performance.

In the current work, numerical simulations are conducted to investigate the effect of the pilot stage FSR on the performance of a single-sector centrally-staged HTR model combustor under a high-power operating condition. With the main and pilot stage swirler structures maintained constant, the flow characteristics of the swirling combustion flow field inside the model combustor, flame morphology development, temperature distribution evolution, and emission characteristics are analysed under various pilot stage FSR. The investigation aims to provide theoretical support and supplement understanding of the performance-influencing mechanisms for a centrally-staged HTR combustor, focusing on a fuel-staging strategy.

2. Geometric model and numerical method

2.1. Geometric model

Fig. 1 shows the swirler structure of the centrally-staged HTR model combustor, which consists of a central pilot stage and a surrounding main stage, equipped with a coaxial axial-flow swirler and a liner without any dilution or cooling holes. In the previous reference [10], the effects of swirling number and direction on flame morphology and combustion performance in the same combustor were investigated. The fundamental structure of the combustor in this work is similar to that described in reference [10]. The two stages of the swirler exhibit clockwise rotation, with the main stage swirler possessing a swirling number of 1.5 and the pilot stage swirler possessing a swirling number of 0.68. The main stage nozzle group is composed of nine nozzles angled at 15° along the axial direction, uniformly distributed circumferentially around the main stage swirler exit. The liner features a rectangular cross-section, an axial length of 210 mm, and a convergent angle of 135°. Kerosene fuel enters the combustor through two-stage fuel nozzles, while air containing oxygen is introduced through the flow channels of two-stage swirlers.
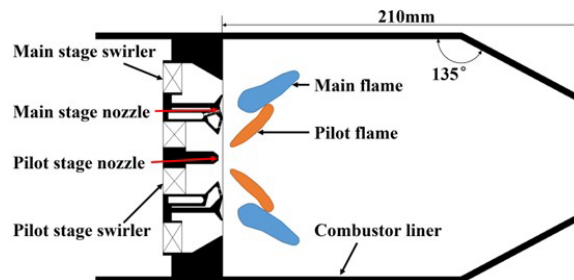

Fig. 1: Structure of centrally-staged HTR model combustor [10].

2.2. Numerical method

Three-dimensional CFD method is used to conduct steady-state RANS [11] calculations. The SIMPLE algorithm is used to resolve the pressure-velocity coupling, while spatial discretization is performed using a second-order discrete scheme. The Realizable k-epsilon turbulence model [12] is employed, with the standard wall function used for near-wall treatment. To account for turbulent combustion, the partially premixed flamelet generated manifold (FGM) mode [13] is chosen, while the discrete particle model (DPM) [14] is used for the multiphase flow. A simplified average molecular

formula $C_{12}H_{23}$ is used instead of aviation kerosene, and diffusion flamelets are generated to parameterize the FGM and construct the PDF table. A 16-species, 23-step kinetic scheme is employed to describe the chemical reactions for Jet-A kerosene. Mass-flow-inlet and pressure-outlet boundary conditions are applied to the inlet and outlet of the combustor, respectively. Table 1 provides the boundary condition parameters of the computational domain as well as the fuel flow rates rates of the main and pilot stages. While maintaining a constant total mass flow rate of fuel, the FSR of pilot stage is systematically adjusted to 10%, 20%. 30%, 40%, 50%, 60%, and 70%.

Table 1: Boundary condition parameters.

Case	m_{air} (kg/s)	P (MPa)	T_{inlet} (K)	m_f (g/s)	FSR
a					10%
b					20%
c					30%
d	0.57	0.4	625	16.4	40%
e					50%
f					60%
g					70%

2.3. Model validation

Fig. 2 compares the velocity distribution at the mid-section of the non-reaction flow field obtained by the numerical simulation with the experimental measurement result from reference [15]. Fig. 3 compares the contours of OH radical distribution obtained by the numerical simulation with the edge of OH fluorescent group distribution obtained from the optical experiment in reaction state (marked with red outline). The numerical simulation results are highly consistent with the experimental results, demonstrating that the numerical simulation method used in this paper accurately captures the combustion flow field structure and is suitable for subsequent research. Given that the independent variable in this work is the FSR, with no modifications made to the combustor structure, the model validation procedure detailed in reference [10] remains applicable to this work.
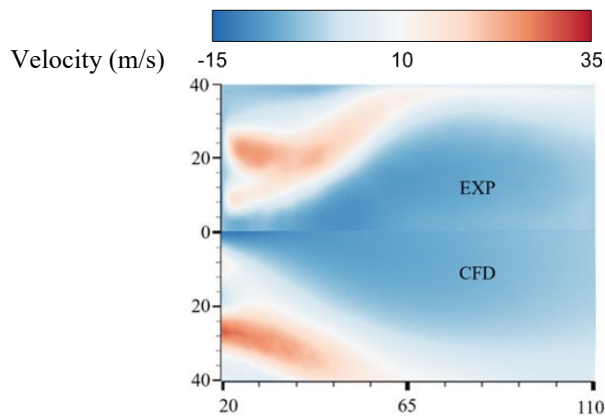

Fig. 2: Comparison on time-averaged axial velocity at mid-section in non-reaction state
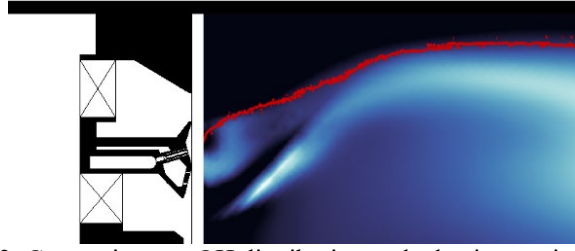between numerical simulation and experimental measurement [10].

Fig. 3: Comparison on OH distribution and edge in reaction state
between numerical simulation and experimental measurement [10].

2.4. Performance Indicator

In the present work, the pattern factor (PF) is used to quantitatively characterize the uniformity of the combustor outlet temperature distribution, as shown in Eq. (1) [16]. The pollutant emissions are converted based on an oxygen concentration of 15%, as shown in Eq. (2) [17]. The total pressure loss coefficient (η_p) and combustion efficiency (η_r) of the combustor are calculated by Eqs. (3) - (4) [18, 19], respectively.

$$PF = \frac{T_{max} - T_{outlet}}{T_{outlet} - T_{inlet}} \times 100\% \tag{1}$$

$$Emissions_{(dry,15\%O_2)} = \frac{(20.9 - 15) \times Emissions_{dry}}{20.9 - O_{2,dry}} \times 10^6 \tag{2}$$

$$\eta_r = \frac{X_{CO_2} + 0.531 X_{CO} - 0.318 X_{CH_4} - 0.397 X_{H_2}}{X_{CO_2} + X_{CO} + X_{UHC}} \times 100\% \tag{3}$$

$$\eta_p = \frac{P_{inlet} - P_{outlet}}{P_{inlet}} \times 100\% \tag{4}$$

Where, T_{inlet} and T_{outlet} denote the average temperature of combustor inlet and outlet, while T_{max} is the maximum outlet temperature, respectively. X_i represents the mole fraction of species such as CO_2, CO, CH_4, H_2, and unburned hydrocarbons (UHC). P_{inlet} and P_{outlet} represent the average pressure of combustor inlet and outlet, respectively.

3. Result and discussion
3.1. Flow field characteristics

Fig. 4 (a) displays the velocity and streamline distribution of the swirling combustion flow field in reaction state when the FSR is 50%. The flow in the two high-speed zones forms inner and outer shear layers (ISL and OSL), while the red solid line representing zero axial velocity delineates the boundary of the recirculation zone. Based on the relative position to the combustor, the recirculation zones can be divided into three categories: the PRZ located near the combustor axis, the lip recirculation zone (LRZ) located in the swirling flow between the main and pilot stages, and the corner recirculation zone (CRZ) located in corners. Fig. 4 (b) compares the distribution of recirculation zones under different FSR values, showing that changes in FSR have little impact on the structure or size of the recirculation zones.

Velocity (m/s)   0   10   20   30   40   50   60   70   80   90   100 110 120 130
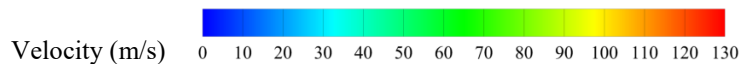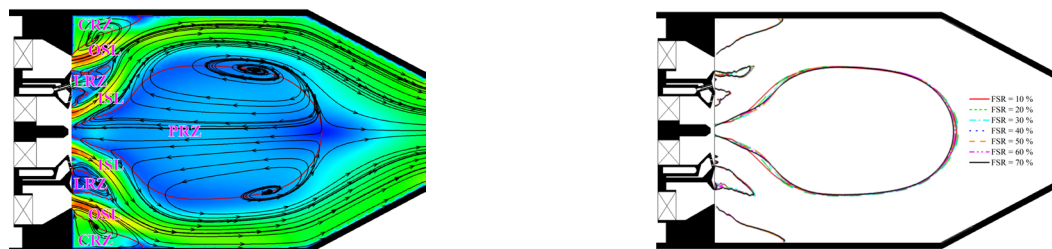
(a) Velocity and streamline distribution (FSR = 50 %) (b) Recirculation zones distribution under different FSR

Fig. 4: Swirling combustion flow field at mid-section.

3.2. Fuel distribution and swirling flame structure

Fig. 5 compares the OH radical and fuel (kerosene) distribution in the mid-section of the combustor under different pilot stage FSR. The grey contour in the upper part represents the mass fraction of OH radical, while the colour contour in the lower part represents the kerosene mass fraction. The fuel exhibits two independent branch structures, with the main and pilot fuel separated by the ISL, indicating distinct fuel stratification between the two stages. The fuel concentration is higher near the pilot stage nozzle exit and lower inside the PRZ, resulting in a distinct V-shaped distribution. For the hydrocarbon fuel, the peak gradient of the OH radical distribution characterizes the flame front position. Based on the OH radical distribution in Fig. 5, the pilot stage flame is located at the edge of the fuel distribution within the PRZ and is stabilized downstream of the pilot stage nozzle. Nine nozzles of the main stage are arranged around the lip, with a significant amount of main fuel distributed downstream, forming a hollow cone structure. Due to lower flow velocity within the LRZ, fuel from the main stage nozzles is directly injected into the LRZ, mixing with swirling air at a state close to the stoichiometric equivalent ratio, thereby distributing the main flame front along the edge of the LRZ. Given that the pilot stage FSR has minimal impact on the LRZ size, different FSR values have little effect on the position of the main flame front. As the pilot stage FSR increases, the axial distance between the pilot flame front and the swirler exit elongates, accompanied by a rise in the pilot fuel mass flow rate. Consequently, the heat release zone of the pilot flame gradually expands and shifts further away from the pilot stage nozzle.
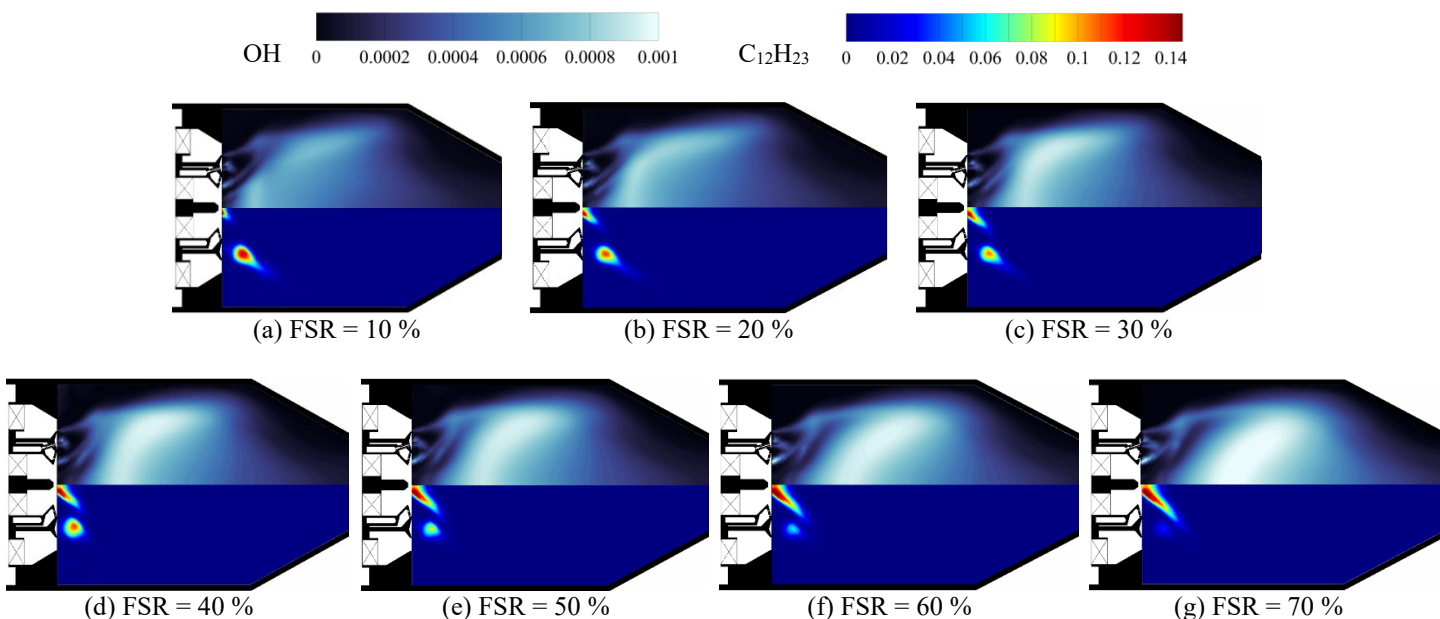

(a) FSR = 10 %   (b) FSR = 20 %   (c) FSR = 30 %

(d) FSR = 40 %   (e) FSR = 50 %   (f) FSR = 60 %   (g) FSR = 70 %

Fig. 5: Comparation between oh and c12h23 mass fraction at mid-section.

3.3. Temperature distribution and combustor performance

Fig. 6 depicts the mid-section temperature distribution in the combustor under different pilot stage FSR. Due to the strong entrainment and backflow effects of the PRZ on high-temperature mixtures, the temperature of the central region within the combustor is significantly higher than that of the CRZ. Inside the PRZ, where the fuel concentration is higher flow velocity is lower, combustion reactions exhibit greater completeness and stability, leading to a higher reaction temperature. Additionally, due to the diffusion flame formed in the pilot stage, the temperature downstream increases significantly. With an increase of pilot stage FSR, the maximum temperature inside the combustor rises, expanding the size of high-temperature zone (T $\geqslant$ 2100K). The increased FSR leads to a significant rise in pilot stage fuel entering the LRZ, resulting in higher local fuel concentration and equivalence ratio within the LRZ, thereby enlarging the high-temperature zone.
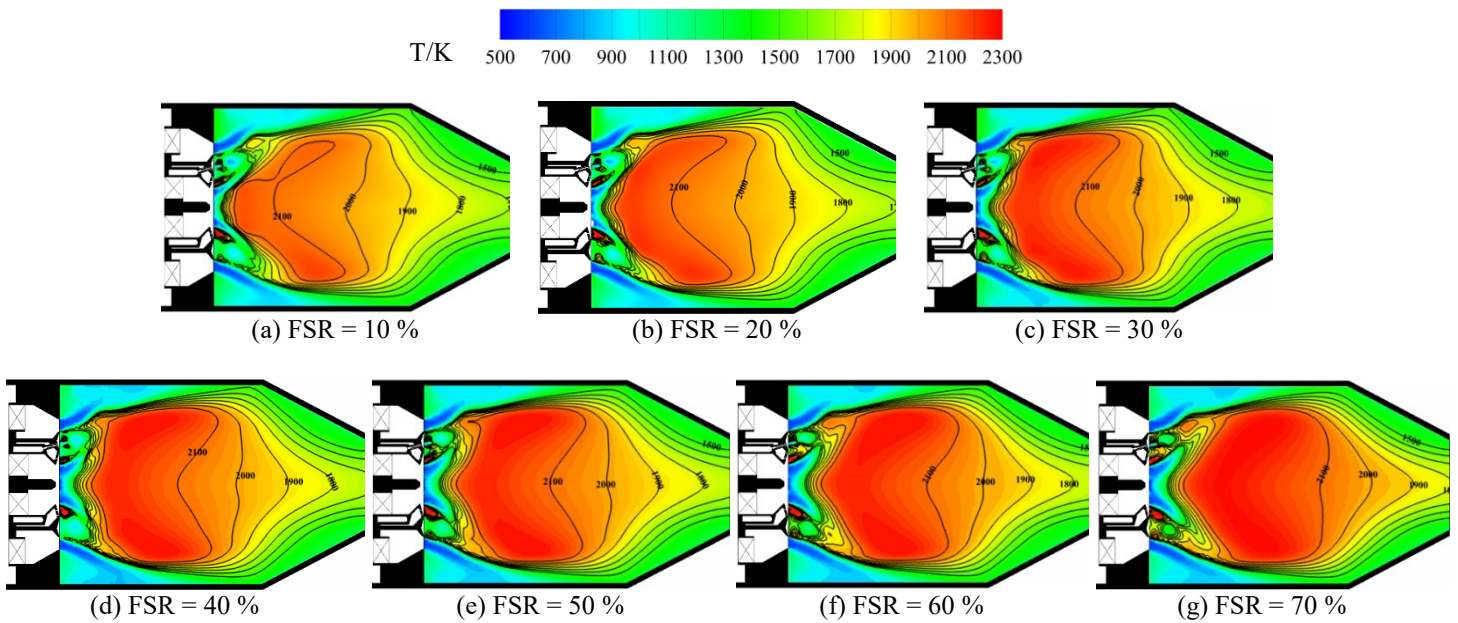

Fig. 6: Temperature distribution at mid-section.

Table 2 presents performance indicators such as combustion efficiency, total pressure loss coefficient, outlet temperature distribution coefficient, and emission indicator of the combustor under various pilot stage FSR. Fig. 7 illustrates the trend of PF and CO emissions (ECO) of the combustor as the FSR varies. The comparison in Fig. 7 clearly demonstrates that variations in pilot stage FSR have a more significant impact on the ECO.

Table 2: Combustor performance indicators.

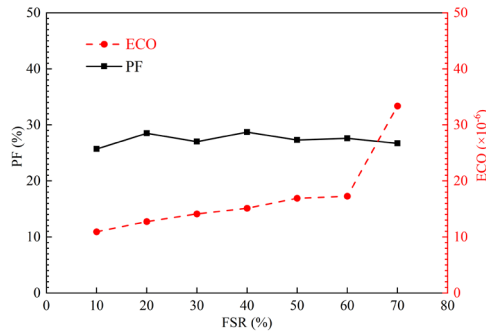| Case	FSR	η_r (%)	η_P (%)	PF (%)	ECO ($\times 10^{-6}$)
a	10%	99.99	4.08	25.7	10.93
b	20%	99.98	4.05	28.5	12.73
c	30%	99.98	4.01	27.0	14.12
d	40%	99.98	3.92	28.7	15.12
e	50%	99.98	3.98	27.3	16.91
f	60%	99.98	3.97	27.6	17.26
g	70%	99.96	4.02	26.7	33.37

Fig. 7: PF and ECO of combustor under various pilot stage FSR.

There is a strong correlation between pollutant emissions and temperature within the combustor. An increase in the mass flow rate of pilot fuel leads to the expansion of the high-temperature zone, consequently increasing the ECO. As the FSR increases to 70%, the ECO sharply increases, exceeding three times that at 10% FSR. The total pressure loss coefficient fluctuates slightly, while the combustion efficiency continues to decline, and the outlet temperature distribution coefficient remains high, indicating a deterioration in overall combustor performance.

4. Conclusion

In this work, numerical simulations investigate the effect of the pilot stage FSR on the performance of a centrally-staged HTR model combustor under high-power operating conditions. With the swirler structure unchanged, the flow characteristics of the swirling combustion flow field, the development of flame morphology, the evolution of temperature distribution, and the emission characteristics are analysed under various pilot stage FSR values. The main conclusions are as follows:

(a) The swirling combustion flow field exhibits three recirculation zones: PRZ, LRZ, and CRZ. Fuel stratification occurs between the main and pilot stages due to ISL influence, resulting in a V-shaped fuel distribution within the combustor.

(b) The flame inside the combustor exhibits layering, with the main flame front located along the edge of the LRZ, minimally affected by variations in the pilot stage FSR. The pilot flame is located at the edge of the fuel distribution contour within the PRZ and stabilizes downstream of the pilot stage nozzle. As the FSR increases, the axial distance between the pilot flame front and the swirler exit elongates, shifting the flame heat release zone further away from the pilot stage nozzle. The maximum temperature inside the combustor rises, and the high-temperature zone exceeding 2100 K expands.

(c) The emission performance of the combustor is significantly affected by variations in the pilot stage FSR. An increase in the pilot stage mass fuel flow rate enlarges the high-temperature zone, resulting in elevated CO emissions.

Acknowledgements

References

[1] Q. H. Zeng and X. W. Chen, "Combustor technology of high temperature rise for aero engine," *Progress in Aerospace Sciences*, vol.140, no. 100927, 2023. https://doi.org/10.1016/j.paerosci.2023.100927.

[2] C. Y. Liu, C. Yang, X. Zhang, H. Li, Y. Liu, D. Q. Feng, "Thermoacoustic coupling characteristics of high-temperature rise combustor", J*ournal of propulsion technology*, vol. 45 (02), no. 2207074, pp. 139-147, 2024. DOI: 10.13675/j.cnki.tjjs.2207074.

[3] L. A. Li, X. Li, Z. Wang, B. Wang, H. J. Lin, W. C. Hu, C. Feng, B. Zhou, "Experimental investigation of the flow-spray field in a realistic concentric staged high-temperature-rise combustor", *Fuel*, vol. 318, no. 123606, 2022. https://doi.org/10.1016/j.fuel.2022.123606.

[4] J. Q. Suo, Y. Han, L. X. Zheng, "Experimental study on lean blowout of a high temperature rise combustor," *55th AIAA Aerospace Sciences Meeting*, Grapevine, Texas, 2017. DOI: 10.2514/6.2017-1056.

[5]   H. Ge, Q. Y. Qin, W. Jin, J. Z. Li, "Large eddy simulation of the influences of the pilot-stage structure on the flow characteristics in a centrally staged high-temperature-rise combustor," *Aerospace*, vol. 9, no. 782, 2022. https://doi.org/10.3390/aerospace9120782.

[6]   K. F. Wang, F. Li, T. Zhou, D. C. Wang, "Numerical simulations on the effect of swirler installation angle on outlet temperature distribution in gas turbine combustors," *Applied Thermal Engineering*, vol. 240, no. 122252, 2024. https://doi.org/10.1016/j.applthermaleng.2023.122252.

[7]   B. L. Sun, W. Y. Song, J. Li, "Study on the influence of fuel supply and distribution on the performance of concentric staged high temperature rise combustor," *Proceedings of ASME Turbo Expo 2022: Turbomachinery Technical Conference and Exposition*, Rotterdam, Netherlands, 2022, vol. 3A: Combustion, Fuels, and Emissions, no. GT2022-81692, V03AT04A045. https://doi.org/10.1115/GT2022-81692.

[8]   S. H. Yang, J. C. Wang, Z. C. Wang, M. Han, Y. Z. Lin, Y. X. Wang, "Experimental investigation of dual-swirl spray flame in a fuel staged optical model combustor with laser diagnostics," *Proceedings of the ASME Turbo Expo 2021: Turbomachinery Technical Conference and Exposition*, Virtual, Online, 2021, vol. 3A: Combustion, Fuels, and Emissions, no. GT2021-58706, V03AT04A015. https://doi.org/10.1115/GT2021-58706.

[9]   T. Z. Zhao, X. Liu, H. T. Zheng, Z. H. Zhang, J. L. Yang, Z. M. Li, "Effect of fuel stage proportion on flame position in an internally-staged combustor," *Proceedings of the ASME Turbo Expo 2020: Turbomachinery Technical Conference and Exposition*, Virtual, Online, 2020, vol. 4A: Combustion, Fuels, and Emissions, no. GT2020-14347, V04AT04A017, 2020. https://doi.org/10.1115/GT2020-14347.

[10] H. H. Xu, Z. F. Li, L. Y. Pang, N. B. Zhao, H. T. Zheng, "Effect of swirling number and direction on flame morphology and combustion performance in a centrally staged swirl combustor," *Proceedings of the ASME Turbo Expo 2024: Turbomachinery Technical Conference and Exposition*, London, United Kingdom, 2024, Vol. 3B: Combustion, Fuels, and Emissions, no. V03BT04A002. https://doi.org/10.1115/GT2024-127266.

[11] Bojan Šekutkovski, Aleksandar Grbovi´c, Ivana Todi´c, Aleksandar Pejˇcev, "A partitioned solution approach for the fluid-structure interaction of thin-walled structures and high-Reynolds number flows using RANS and hybrid RANS-LES turbulence models," *Aerospace Science and Technology*, vol. 113, no. 106629, 2021. https://doi.org/10.1016/j.ast.2021.106629.

[12] R. M. Zhao, S. M. Liu, J. J. Liu, N. Jiang, Q. Y. Chen, "Equation discovery of dynamized coefficients in the k-ε model for urban airflow and airborne contaminant dispersion," *Sustainable Cities and Society*, vol. 99, no. 104881, 2023. https://doi.org/10.1016/j.scs.2023.104881.

[13] F. S. Almutairi, K. K. J. Ranga Dinesh, J. A. van Oijen, "Modelling of hydrogen-blended dual-fuel combustion using flamelet-generated manifold and preferential diffusion effects," *International Journal of Hydrogen Energy*, vol. 48, no. 4, pp. 1602-1624, 2023. https://doi.org/10.1016/j.ijhydene.2022.10.078.

[14] N. M. Zahari, M. H. Zawawi, L. M. Sidek, Daud Mohamad, Zarina Itam, M. Z. Ramli, Agusril Syamsir, Aizat Abas, M. Rashid, "Introduction of discrete phase model (DPM) in fluid flow: A review," AIP Conf. Proc, 2030, 020234, 2018. https://doi.org/10.1063/1.5066875.

[15] X. Z. Feng, J. Q. Suo, P. F. Zhu, Y. Li, Q. D. Li, "Numerical study of flow characteristics of a central-staged swirl combustor," Proceedings of ASME Turbo Expo 2022: Turbomachinery Technical Conference and Exposition, Rotterdam, Netherlands, 2022, vol. 3A: Combustion, Fuels, and Emissions, no. GT2022-81552, V03AT04A038. https://doi.org/10.1115/GT2022-81552.

[16] M. M. Torkzadeh, F. Bolourchifard, E. Amani, "An investigation of air-swirl design criteria for gas turbine combustors through a multi-objective CFD optimization," Fuel, vol. 186, no. 734-749, 2016. https://doi.org/10.1016/j.fuel.2016.09.022.

[17] A. H. Lefebvre, D. R. Ballal, Gas turbine combustion: alternative fuels and emissions, New York, CRC Press, 2010.

[18] H. G. Zhong, H. H. Ji, J. B. Li, "Methods for gas temperature measurement by gas analysis," Journal of Aerospace Power, vol. 20, no. 3, pp. 460-466, 2005. (In Chinese).

[19] L. Yu, X. He, Q. Hong, Y. Guo, P. Zhang, "Effect of primary hole parameters on combustor performance within a slinger combustor," Applied Thermal Engineering, vol. 216, no. 119038, 2022.